Supporting Information: Elucidating the Interplay Between Entropy-Driven and Patch-Mediated Bonding in Directing Nanoscale Assemblies

Kireeti Akkunuri[1†], Xiangyu Zhang[1†], Thi Vo[1*]

[1] Chemical and Biomolecular Engineering, Johns Hopkins University, Baltimore, MD 21218

† Equal contributions

* Corresponding Author: tvo12@jhu.edu

Contents

Appendix A: Shape Orbitals for Connectivity Generalization of Entropic Bonding Theory

Here, we provide details for the generalization of entropic bonding theory (EBT) to account for the connectivity between different surface locations on the particle. EBT has the following form

$$\beta U_m(r) = r^{-2}\left[\ln \rho_{pP}(r) - \beta\mu_{pP}\right] + \sum_i^N \beta U_{core}(r) \tag{A.1}$$

$$\left[\nabla^2 + \beta\nabla^2 U_m - \left(\beta\nabla U_m\right)^2\right]\rho_{pP} = E\rho_{pP} \tag{A.2}$$

where r is the pP-NP center-to-center separation, ρ_{pP} and μ_{pP} are the density distribution and chemical potential of pPs, respectively, and $\beta = 1/kT$. $U_{core}(r)$ is a hard-core repulsion between pPs and NPs. Solving for the shape orbitals using **Eq. A.1 – A.2** employs both of separations of variables and power law series expansions that ultimately yields[1]:

$$\begin{gathered} S(u) = \sum_{j=0}^{l-1} a_j\left[\Gamma_u(u)\right]^j \\ \Gamma_u(u) = \cos^4(u) + \sin^4(u) \\ a_{j+1} = \frac{a_j[(j+1)(j+1/2)] - 2a_{j-1}\left[l^2 - j^2\right]}{(j+1)(j+2)} \end{gathered} \tag{A.3}$$

$$\begin{gathered} S(v) = \sum_{j=0}^{k-1} a_j\left[\Gamma_v(v)\right]^{2j} \\ \Gamma_v(v) = \cos(v), \quad |k| < 2(l-1) \\ \frac{a_{j+1}}{a_j} = \frac{(2\Omega)^{-1}\left[16l^2 - 4(k+1)^2\right]}{(k+1)^2 - (j+1)^2} \end{gathered} \tag{A.4}$$

$$\begin{gathered} S(w) = w^{K_{pp}} e^{\left(-\frac{2\Omega^2 Bw}{n}\right)} \sum_{j=0}^{n_m} a_j w^j \\ \frac{a_{j+1}}{a_j} = \left(\frac{4\Omega^2 B}{n}\right)\left[\frac{j + K_{pp} + 1 - n}{(j+1)\left(2K_{pp} + 2 - j\right)}\right] \end{gathered} \tag{A.5}$$

$$\begin{gathered} n_m = 2n - \sqrt{4K_p + 1} - 1 \\ K_p = 4\Omega\left[4l^2 - (k+1)^2\right] \\ K_{pp} = 2^{-1}\left(\sqrt{4K_p + 1} - 1\right) \end{gathered} \tag{A.6}$$

where u, v, w are generalized coordinate variables and are analogous to θ, ϕ, and r in spherical coordinates. l, k, and n are the corresponding power law series exponents analogous to l, m, and n from the general solution to Laplace's equation in spherical coordinates. Ω defines the distance from the surface of the NP to its center, normalized by the smallest surface-to-center distance for each respective shape. Note that Ω is dependent on the surface location of the NP. For example, $\Omega = 1, \sqrt{2}$, and $\sqrt{3}$ for the face, edge and corner location of a cube, respectively. B is a prefactor that correlates with the magnitude of pP-NP interaction at different values of μ_{pP}. The solution ρ_{pP} is simply the product of **Eqs. A.3 – A.6**: $\rho_{pP} = S(u)S(v)S(w)$. This is derived in detail in the original EBT manuscript[1]. While **Eqs. A.3 – A.6** are complex, recasting the generalized coordinates into geometries commensurate with the NP shape of interest drastically simplifies the set of solutions and bypasses the need to consider higher order terms in the series solutions. Specifically, EBT has been shown to accurately capture emergent directional interactions between anisotropic particles as well as their assembly behaviors in the "zeroth order" limit of $l = 1$, $n_m = 0$, and $k = 0$. This simplifies the solution for ρ_{pP} to be $\rho_{pP}(w) = w^{K_{pp}e^{\left(-\frac{2\Omega^2 Bw}{n}\right)}}$ as both $S(u)$ and $S(v)$ terms reduce to constants.

Borrowing from these findings, we apply the same simplification to the connectivity generalization (cEBT). As indicated in the main text, our approach creates a composite set of particles to represent each patchy NP in the system: one core, polyhedral particle to represent NP geometry and a set of spherical particles placed at their corresponding surface locations to represent the patches. Through this lens we can write the composite ρ_{pP} as.

$$\rho_{pP}(r) = r^{K_{pp}e^{\left(-2\Omega^2 Br\right)}} + \sum_{i=1}^{M}\sum_{m} r^{K_{pp,o}e^{\left(-2Br_p + B\delta_m k_h [r_p - r_o]^2\right)}_{p}} \qquad \text{(A.7)}$$

The first term in **Eq. A.7** accounts for the effect of the NP core as a function of distance away from the NP's center. The second term in **Eq. A.7** accounts for contribution from all M patches on the NP. The interior summation within the second term accounts for the effect of connectivity, where contribution from the harmonic-like bonding potential only applies between bonds existing in the set of m bonds within the system (as indicated by the Kronecker δ_m). The variable r_p defines the relative distance to the patch from the core NP frame of reference. As a final note, while **Eq. A.7** appears to be purely radially dependent, there is an implicit angular dependence as well built into Ω which takes on different values for different surface location on the core NP. For the second set of term in **Eq. A.7**, patches are assumed to be spherical, thus $\Omega = 1$ across all patch particles. Similarly, $K_{pp,o}$ reflects the same limit of $\Omega = 1$ in K_{pp} (**Eq. A.6**). The composite ρ_{pP} is then coupled to **Eq. A.2** and solved self-consistently to determine the free energy of all relative orientations between patchy NPs as well as polymeric NPs discussed in the main text.

Appendix B: Scaling Relationship for Anisotropic Polymers

Here, we derive the scaling relationship for anisotropic polymer from the main text (**Eq. 6**). We start by defining the following conditions for a random walk where there are uneven steps along the left versus right direction.

$$N = n_L + n_R \tag{B.1}$$

$$R = \lambda_L n_L - \lambda_R n_R \tag{B.2}$$

where N is the total number of steps, and n_L and n_R are the number of left and right steps, respectively. λ_L and λ_R are the displacement taken per left versus right step, respectively, and R is the net displacement after N total steps. In the limit of $\lambda_L = \lambda_R = 1$, **Eq. B.2** converges to the classical random walk limit. Rearranging **Eqs. B.1** and **B.2** to define the n_L and n_R in terms of N, R, λ_L, and λ_R yields:

$$n_L = \frac{\lambda_R N + R}{\lambda_L + \lambda_R} \tag{B.3}$$

$$n_R = \frac{\lambda_L N - R}{\lambda_L + \lambda_R} \tag{B.4}$$

Eqs B.3 and **B.4** now readily plugs into the binomial distribution to define the probability of having a displacement R:

$$P(R) = \frac{N!}{n_L! n_R!}\left(\frac{1}{2}\right)^N \tag{B.5}$$

Taking the natural log of each side, applying Stirling's approximation ($\ln N! \sim N\ln N - N$), and grouping terms eventually yields:

$$\ln P(R) = N\ln\left[\left(\frac{\lambda_L + \lambda_R}{2}\right)\left(\frac{1}{\lambda_R^{\lambda_R}\lambda_L^{\lambda_L}}\right)^{(\lambda_L + \lambda_R)^{-1}}\right] \tag{B.5}$$

$$+\left[\frac{R}{\lambda_L+\lambda_R}\right]\left[\ln\left(\frac{\lambda_L}{\lambda_R}\right)+\lambda_L-\lambda_R\right]+\left[\frac{R^2}{2N}\right]\left[\frac{\lambda_L+\lambda_R-4}{\lambda_L+\lambda_R}\right]$$

as a consistency check, in the limit of $\lambda_L=\lambda_R=1$, the first and second term in **Eq. B.5** converge to 0 and we get:

$$\ln P(R) = -\frac{R^2}{2N} \tag{B.6}$$

which is the classical result for the idealized random walk. For convenience, we define the following:

$$\Gamma=\left(\frac{\lambda_L+\lambda_R}{2}\right)\left(\frac{1}{\lambda_R^{\lambda_R}\lambda_L^{\lambda_L}}\right)^{(\lambda_L+\lambda_R)^{-1}}$$

$$a=-\left[\frac{\ln\left(\lambda_L/\lambda_R\right)+\lambda_L-\lambda_R}{\lambda_L+\lambda_R}\right]$$

$$b=-\left[\frac{\lambda_L+\lambda_R-4}{2N(\lambda_L+\lambda_R)}\right]$$

Using the above definition and taking the exponential of both sides in **Eq. B.6** yields:

$$P(R)=\Gamma^N e^{-aR-bR^2} \tag{B.7}$$

Enforcing that the integral over all space of **Eq. B.7** must equal 1 and solving for the corresponding normalization constant results in the generalized random walk probability distribution:

$$P(R)=\left(\frac{b}{\pi}\right)^{1/2} e^{-a^2/4b}\, e^{-aR-bR^2} \tag{B.8}$$

Integrating **Eq. B.8** to obtain the average squared displacement $\langle R^2\rangle$ gives

$$\langle R^2\rangle=\left(\frac{1}{8}\right)\left\{4N^2\left[\frac{\ln\left(\lambda_L/\lambda_R\right)+\lambda_L-\lambda_R}{\lambda_L+\lambda_R-4}\right]^2-4N\left[\frac{\lambda_L+\lambda_R}{\lambda_L+\lambda_R-4}\right]\right\} \tag{B.9}$$

Again, as a consistency check, **Eq. B.9** converges to $\langle R^2\rangle=2^{-1}N$, which is the classical ideal random walk result. Taking the 3D limit of **Eq. B.8** and solving for $\langle R^2\rangle$ results in:

$$\langle R^2\rangle=4^{-1}\sum_{i\,\epsilon\,\{x,y,z\}}4N^2\left[\frac{\ln\left(\lambda_L/\lambda_R\right)+\lambda_L-\lambda_R}{\lambda_L+\lambda_R-4}\right]_i^2-4N\left[\frac{\lambda_L+\lambda_R}{\lambda_L+\lambda_R-4}\right]_i \tag{B.10}$$

We now simplify **Eq. B.10** to derive the scaling relationship defined in **Eq. 6** of the main text. Firstly, we define a scaled step size relative to a rightward step: that is, $\lambda_R \sim 1$ and $\lambda_L \epsilon [0,1]$. Note that the derivation of **Eq. B.1 – B.10** can choose to factor out λ_L instead of λ_R. This will flip ratio terms of the form λ_L/λ_R that appears in the above equations, allowing for the opposing choice of $\lambda_L \sim 1$ and $\lambda_R \epsilon [0,1]$. In other words, the system is symmetric. Applying this definition reduces the numerator of bracketed term associated with N^2 term in **Eq. B.10** to:

$$\ln\left(\lambda_L/\lambda_R\right) + \lambda_L - \lambda_R = \left[\ln \lambda_L\right]^2 \left[1 + \frac{\lambda_L - 1}{\ln \lambda_L}\right]^2 \tag{B.11}$$

To a first order approximation, $\frac{\lambda_L - 1}{\ln \lambda_L} \sim \lambda_L^{1/2}$ for $\lambda_L \epsilon [0,1]$. Plugging this approximation into **Eq. B.11** yields:

$$\left[\ln \lambda_L\right]^2 \left[1 + \frac{\lambda_L - 1}{\ln \lambda_L}\right]^2 \sim \left[\frac{\lambda_L - 1}{\lambda_L^{1/2}}\right]^2 \left[1 + \lambda_L^{1/2}\right]^2 \tag{B.12}$$

Combining **Eq. B.12** with the denominator of the bracketed term associated with N^2 results in

$$\left[\frac{1}{\lambda_L}\right] \left[\frac{\lambda_L - 1}{\lambda_L - 3}\right]^2 \left[1 + \lambda_L^{1/2}\right]^2 \tag{B.13}$$

By inspection, **Eq. B.13** scales as $\lambda_L^{-1} - 1$ for $\lambda_L \epsilon [0,1]$. Simplifying **Eq. B.10** with the approximated expression yields

$$\langle R^2 \rangle = \sum_{i \epsilon \{x,y,z\}} N^2 \left[\frac{1}{\lambda_L} - 1\right]_i^2 - N \left[\frac{\lambda_L + 1}{\lambda_L - 3}\right]_i \tag{B.14}$$

The term associated with N is of unitary order (-1) for small values of λ_L, thus we can approximate **Eq. B.10** to be

$$\langle R^2 \rangle \sim N^2 \left[\frac{1 - \lambda_{L,x}}{\lambda_{L,x}} + \frac{1 - \lambda_{L,y}}{\lambda_{L,y}} + \frac{1 - \lambda_{L,z}}{\lambda_{L,z}}\right] + N \tag{B.15}$$

where $\lambda_{L,x}$, $\lambda_{L,y}$, and $\lambda_{L,z}$ defined the scaled leftward displacement (assuming $\lambda_R \sim 1$). For 3D systems, we are interested in the composite product $\lambda_{L,x}\lambda_{L,y}\lambda_{L,z}$. Rearranging the bracketed terms in **Eq. B.15** yields

$$\frac{\lambda_{L,x}\lambda_{L,y} + \lambda_{L,x}\lambda_{L,z} + \lambda_{L,y}\lambda_{L,z} - 3\lambda_{L,x}\lambda_{L,y}\lambda_{L,z}}{\lambda_{L,x}\lambda_{L,y}\lambda_{L,z}} \tag{B.16}$$

Since each λ_L ranges between 0 and 1, the double product terms are generally larger than the triple product terms: $\lambda_{L,x}\lambda_{L,y} \gg \lambda_{L,x}\lambda_{L,y}\lambda_{L,z}$, with a max possible value of 1. As such we can take the approximation that the double product terms are of unitary order relative to the triple product term:

$$\frac{1-\lambda_{L,x}}{\lambda_{L,x}} + \frac{1-\lambda_{L,y}}{\lambda_{L,y}} + \frac{1-\lambda_{L,z}}{\lambda_{L,z}} \sim \frac{1-\lambda_{L,x}\lambda_{L,y}\lambda_{L,z}}{\lambda_{L,x}\lambda_{L,y}\lambda_{L,z}} \tag{B.17}$$

The triple product term $\lambda_{L,x}\lambda_{L,y}\lambda_{L,z}$ essentially represents the product of the biased step sizes along a 3D path (on a lattice) that a random walker can take. On the surface of an anisotropic particle, this is equivalent to the product of the differential step that a trajectory can take. Locations of higher curvature will exhibit larger values relative to lower curvature surface sites. For example, a face location on a cube will have the lowest value of $\lambda_{L,x}\lambda_{L,y}\lambda_{L,z}$ (in fact, $\lambda_{L,x}\lambda_{L,y}\lambda_{L,z} = 0$) since it is not possible to step backwards into the face of a cube. Conversely, $\lambda_{L,x}\lambda_{L,y}\lambda_{L,z}$ is largest at the vertex of the cube since it can freely step only any direction without experiencing any confinement: $\lambda_{L,x}\lambda_{L,y}\lambda_{L,z} = 1$. For this reason, we define a parameter Λ that corresponds to a scaled surface-to-center distance for any anisotropic particle. $\Lambda \in [0,1]$ and is defined such that the vertex furthest away from the particle's center is set to 1 and the location corresponding to the center of the particle's largest face is set to 0. For the case of a spherically symmetric particles, $\Lambda = 1$ for all surface locations. This parameterization allows us to map the discrete lattice steps from the random

walk derivation to the surface of any arbitrarily shaped particle: $\frac{1-\lambda_{L,x}\lambda_{L,y}\lambda_{L,z}}{\lambda_{L,x}\lambda_{L,y}\lambda_{L,z}} \sim \frac{1-\Lambda}{\Lambda}$. To simplify **Eq. B.15** to form more analogous to traditional polymer scaling theory, we first define the convenience term $\Gamma_{eff}^{-1} = \Lambda_{eff} = \Lambda^{-1}(1-\Lambda)$. Introducing this to **Eq. B.15** and setting the right-hand side equal to N^{ν} yields:

$$\langle R^2 \rangle \sim N^{\nu} \sim N^2 \Gamma_{eff}^{-1} + N \tag{B.18}$$

Solving **Eq. B.18** for the exponent ν gives:

$$\nu \sim 1 + [\ln N]^{-1} \left[\ln\left(1 + N/\Gamma_{eff}\right)\right] \tag{B.19}$$

We can apply L'Hopital's Rule to the second term on the right-hand side of **Eq. B.19** to obtain:

$$\nu \sim 1 + N\left(N + \Gamma_{eff}\right)^{-1} \tag{B.20}$$

Plugging in that $\Gamma_{eff}^{-1} = \Lambda_{eff}$ and simplifying gives:

$$\nu \sim 1 + \Lambda_{eff} N\left(\Lambda_{eff} N + 1\right)^{-1} \tag{B.21}$$

As a final step, we note that $\Lambda_{eff} N\left(\Lambda_{eff} N + 1\right)^{-1}$ scales analogously to $\alpha\Lambda_{eff}\left(\Lambda_{eff} + 1\right)^{-1}$ where α is an undetermined multiplier that will be solved to match with known scaling behaviors for ν. Making this approximation and plugging this into **Eq. B.21** gives

$$\nu \sim 1 + \alpha\Lambda_{eff}\left(1 + \Lambda_{eff}\right)^{-1} \tag{B.22}$$

Lastly, we plug-in $\Lambda_{eff} = \Lambda^{-1}(1-\Lambda)$ and simplify to get:

$$\nu \sim (1-\alpha) + \alpha\Lambda \tag{B.23}$$

For the case of a face-face bonded anisotropic particle (i.e. face-face connected cubes) we know that the scaling behavior is rigid-rod-like ($\nu = 2$). Here, $\Lambda = 0$ and solving for α yields, $\alpha = -1$.

Alternatively, one can choose to match exponent for the gaussian limit $\nu = 1$ for $\Lambda = 1$. However, this will result in the trivial solution of $\alpha = \alpha$ and thus is not useful for to determine the value of the undetermined multiplier. Plugging α into **Eq. B.18** yields

$$\langle R^2 \rangle \sim N^{2-\Lambda} \tag{B.24}$$

or, in a more recognizable form:

$$\langle R^2 \rangle^{1/2} \sim N^{(2-\Lambda)/2} \tag{B.25}$$

Eq. B.25 is what is reported in the main text. As a final consistency check. Our parameterization of Λ converges to Λ in the limit of either a spherical particle or a sharp vertex for any anisotropic shape. Vertex-vertex connected particles freely sweep out their circumsphere and thus behave akin to spherical particles. In both these cases, **Eq. B.25** predicts that the scaling relationship converges to $\langle R^2 \rangle^{1/2} \sim N^{1/2}$, which is the classical result for a gaussian polymer chain. This indicates that the derived relationship for end-to-end distance of polymeric chains with anisotropic monomers converges to the well-established spherical bead-spring behaviors.

Appendix C: Model Validation for Spherical Monomeric Subunits

To ensure that our patchy models can reproduce known chain conformational behaviors for polymers composed of spherically symmetric monomers, we first characterize the patchy sphere systems and measure the end-to-end scaling exponent v ($R \sim N^{v}$) for small ($r_o = 0.1\sigma_{in}$), medium ($r_o = 1.0\sigma_{in}$)and large ($r_o = 5.0\sigma_{in}$) patch sizes.

Harmonic Bonding Potential: In the limit of large patches, monomers are so far apart that they do not feel the presence of their bonded neighbors, resulting in the well-known gaussian scaling behavior: $v = 0.53 \pm 0.04$. Reduction of the to medium patch sizes brings particles close together and within range of excluded volume interactions between neighbors. This results in a self-avoiding walk behavior (good solvent), yielding the classical scaling exponent of $v = 0.59 \pm 0.02$. Further decreases in bond length to small patch sizes produces a stiff bond where particles cannot rotate freely, resulting a high degree of chain extension with scaling exponent of $v = 0.70 \pm 0.03$. This high level of rigidity reflects the colloidal polymer limit where bonds are inflexible as the patches mediating bond formation are small compared to the core particle size. Results from **Fig. D1** for patchy spheres indicate that our MC model can reproduce the known behaviors for traditional polymers and can systematically be employed to explore both ideal and self-avoiding chain conformations.

FENE Bonding Potential: The chain lengths considered for these simulations are N = 40, 50, 60, 70, 80, 90, 100, 110, 120, 140, 150, 160, 170, 180, 190, 200. The particles are defined as spheres of $\sigma = 40$, connected by FENE-WCA bonds with parameters $k = 30,\ r_0 = 1.725\sigma$, analogous to the bonds defined between patches in the anisotropic-monomer counterparts. The simulation is performed in an NVT ensemble (implicit-solvent), and run at a temperature of $k_B T = 0.9$. Monomers not bonded to each other repel each other as hard particles through the WCA potential.

The integration step-size is $dt = 0.001$ simulation time units. The simulation is run for a total of 50,000 simulation time units, from which long-time scaling statistics are computed and averaged across 3 distinct runs. Measured scaling exponents from FENE potential simulations for a single chain of spherical monomers connected yield a scaling exponent of 0.61 ± 0.01.

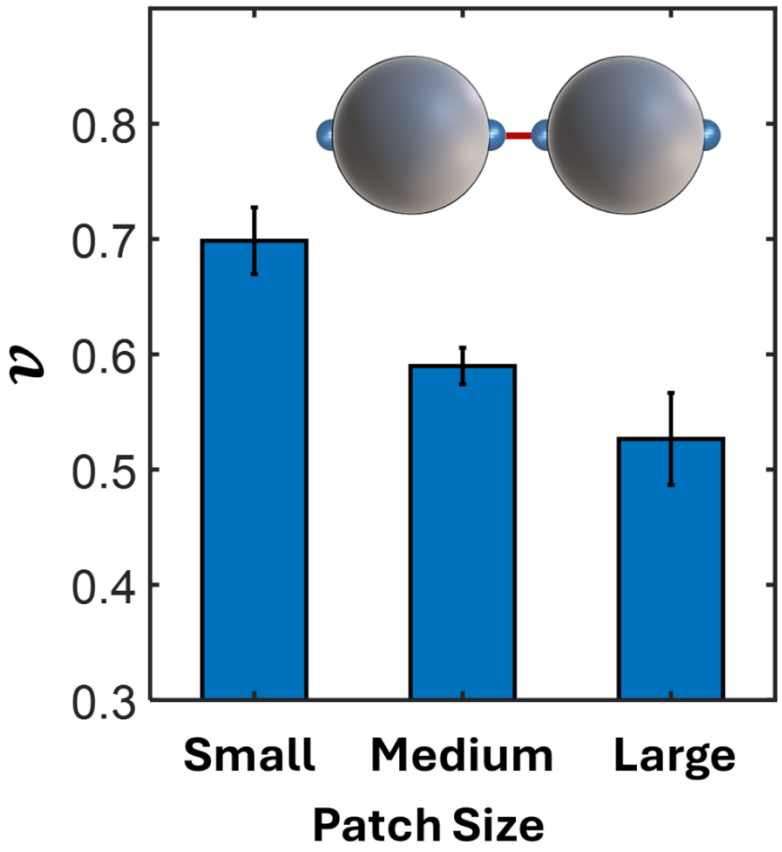

Figure D1. Polymer with Spherical Monomeric Subunits. End-to-end distance scaling exponent ν ($R \sim N^{\nu}$) for chains constructed from patchy spheres with different patch sizes. We observe a transition from rod-like to self-avoiding to ideal chain behaviors with increasing patch sizes. Inset show schematic of bond location and bond length definition for patchy spheres. Bond locations are represented by blue spheres.

Appendix D: cEBT Calculations for 2D Squares, Pentagon, and Hexagons

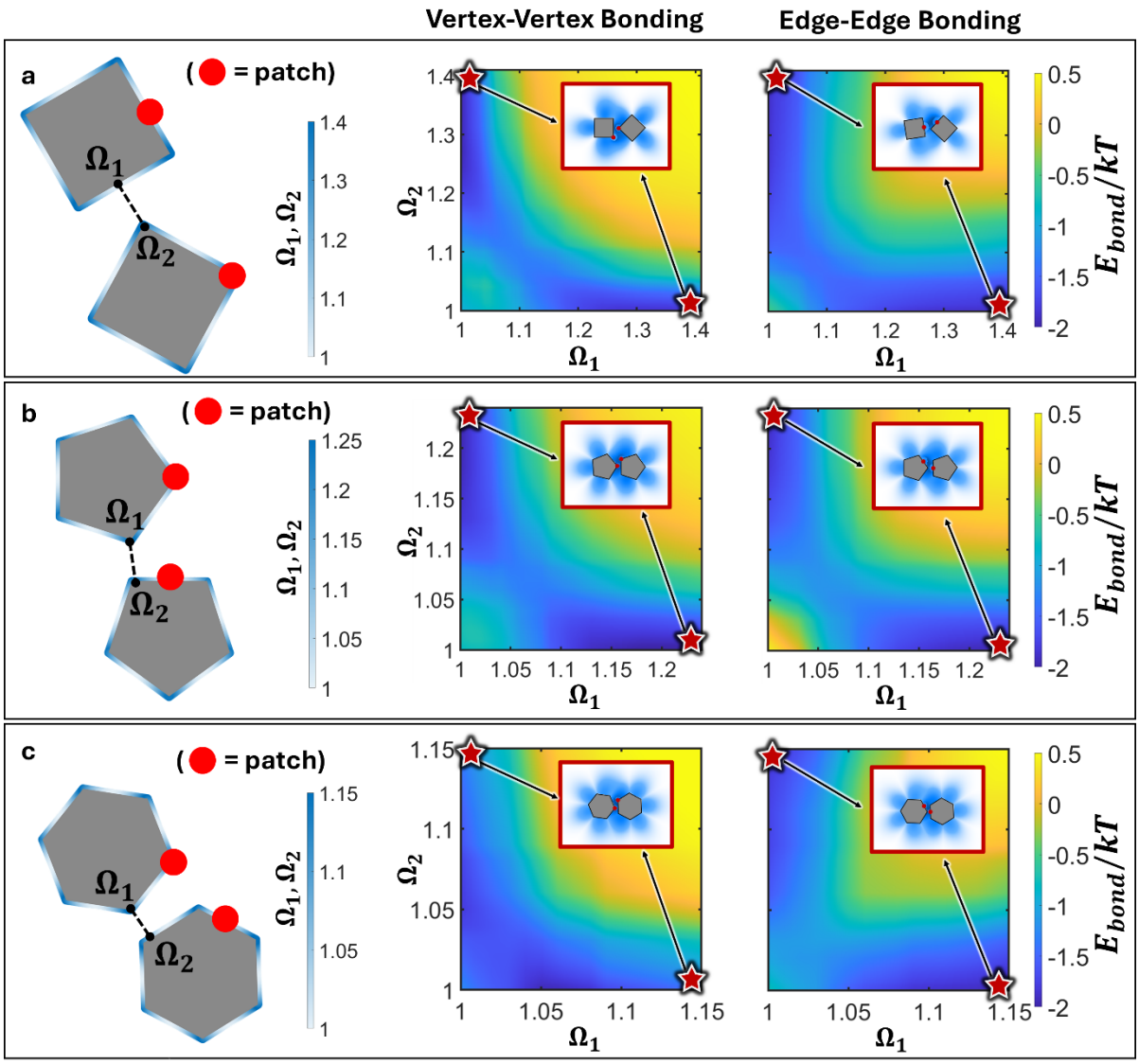

Figure D1. cEBT Energy Surface for 2D Polygons. a) Square, b) pentagon, and c) hexagon. Relative orientations between two shapes are indicated by the closest point of contact on the surface of each respective triangle (indicated by shape factors Ω_1 and Ω_2). Red points indicate the patch location. Free energy surface for edge-edge and vertex-vertex connected polygons with patch size of $0.15^{S_{NP}}$. All results indicate that a non-trivial vertex-edge motif is the thermodynamically stable configuration, breaking away from both the expected tip-tip and edge-edge relative orientational ordering. All insets plot the lowest energy configuration between the bonded triangles and red stars indicate the location of the stable configuration on the free energy landscape.

Appendix E: cEBT Calculations for 3D Octahedra and Tetrahedra

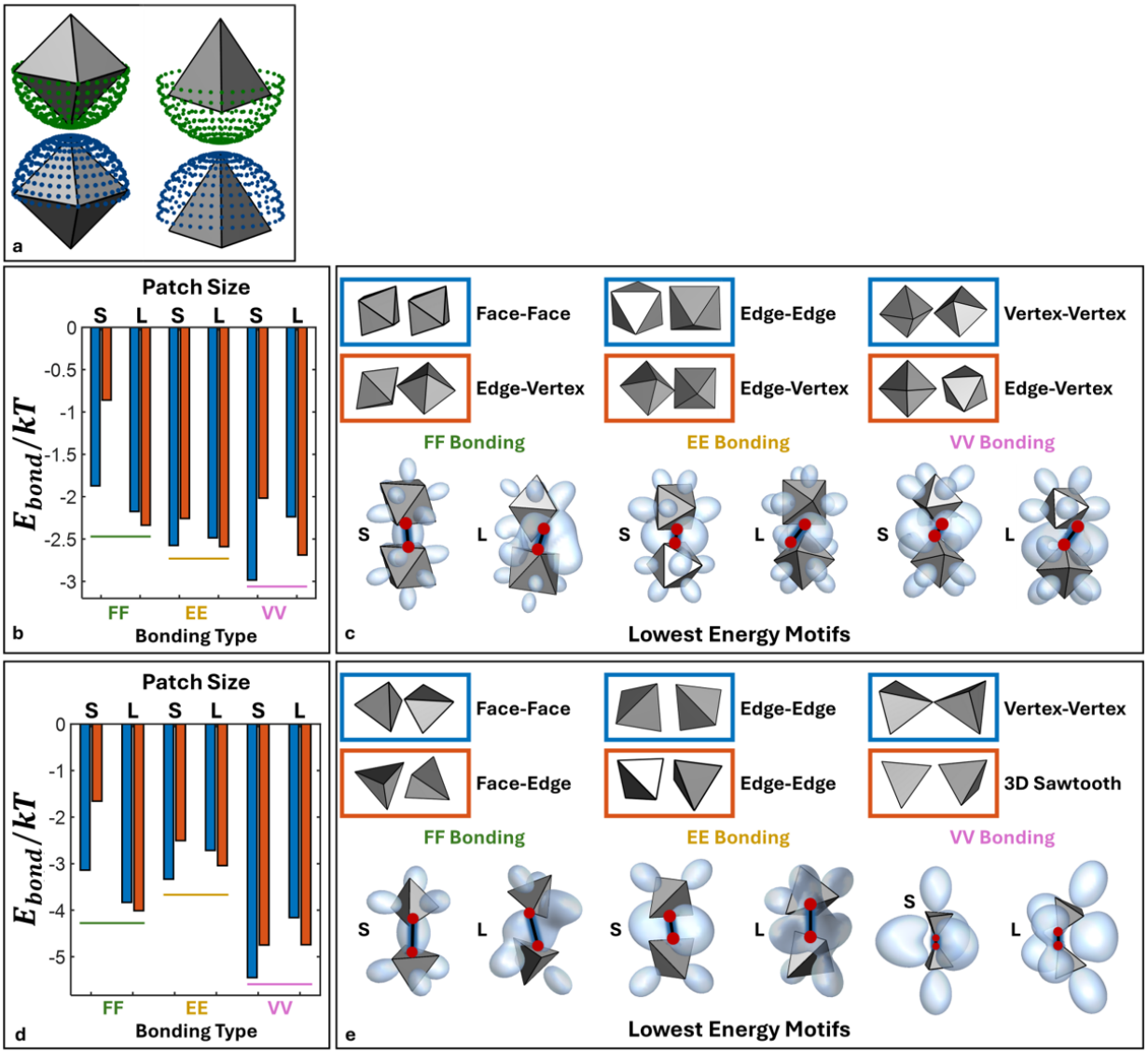

Figure E1. cEBT Prediction for 3D Octahedra and Tetrahedra. a) All pairwise relative orientations indicated are computed in cEBT calculations. Equilibrium predictions are shown for small (S) and large (L) patches b) octahedra and d) tetrahedra for face-face, edge-edge, and vertex-vertex connectivity. Visualization of the bonding orbitals are shown in c) for octahedra and e) for tetrahedra. In all cases, the lowest energy configuration and E_{bond} are visualized and compared between small patches and large patches (analogous in style to **Fig. 3** in main text).

Appendix F: Simulation Snapshots and Scaling for Polymers with Octahedral Subunits

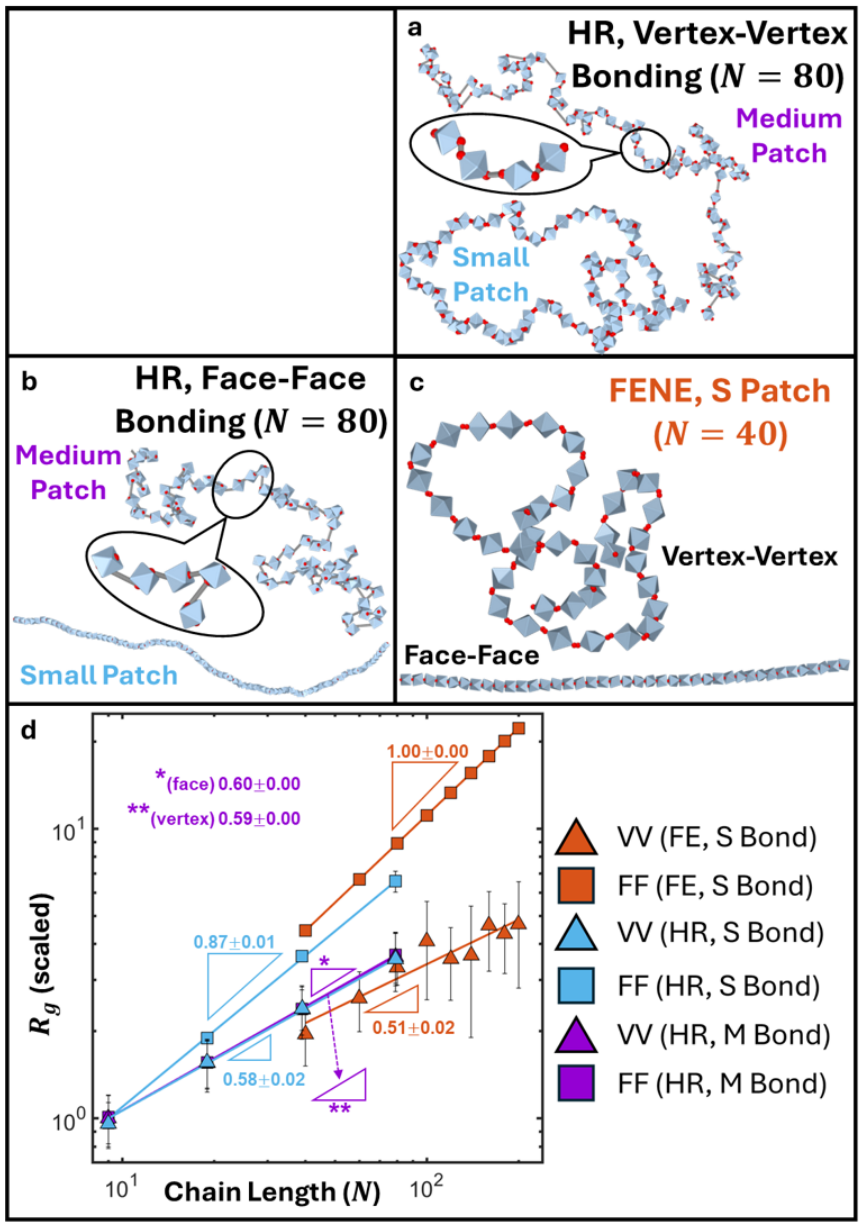

Fig. F1. Polymers with Octahedral Monomeric Subunits. Simulation snapshots of harmonically bonded octahedral NPs for small and medium patch sizes for a) vertex-vertex bonded NPs and b) face-face bonded NPs. c) Simulation snapshot of FENE bonded octahedral NPs (small patch size) for both face-face and vertex-vertex bonding. d) R_g vs N scaling fits for face-face and vertex-vertex bonded polymeric chain of octahedra for small and medium patch sizes across both FENE and harmonic (HR) bonding potential simulations.

Appendix G: Simulation Snapshots and Scaling for Polymers with Tetrahedral Subunits

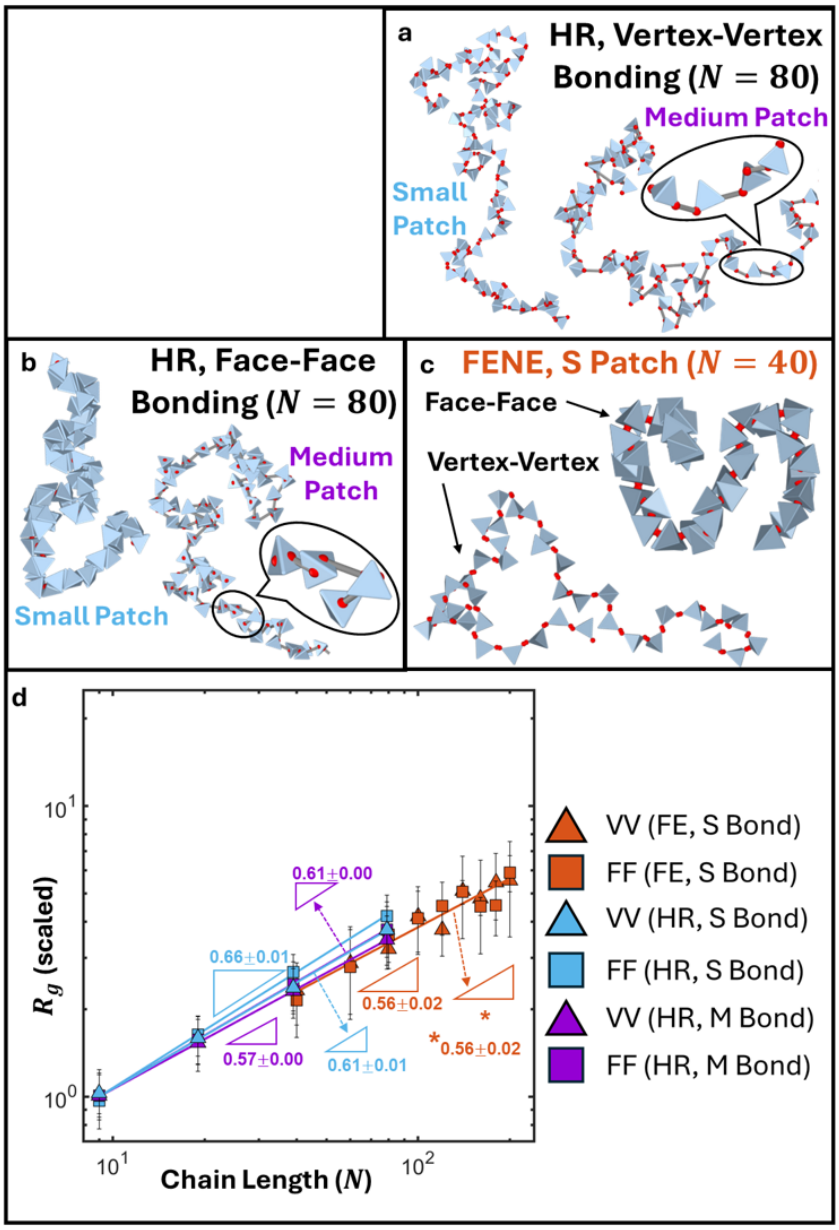

Fig. G1. Polymers with Tetrahedral Monomeric Subunits. Simulation snapshots of harmonically bonded tetrahedral NPs for small and medium patch sizes for a) vertex-vertex bonded NPs and b) face-face bonded NPs. c) Simulation snapshot of FENE bonded tetrahedral NPs (small patch size) for both face-face and vertex-vertex bonding. d) R_g vs N scaling fits for face-face and vertex-vertex bonded polymeric chain of tetrahedra for small and medium patch sizes across both FENE and harmonic (HR) bonding potential simulations.

Appendix H: FENE Simulation Snapshots and Scaling for Edge-Edge Bonded Polymers

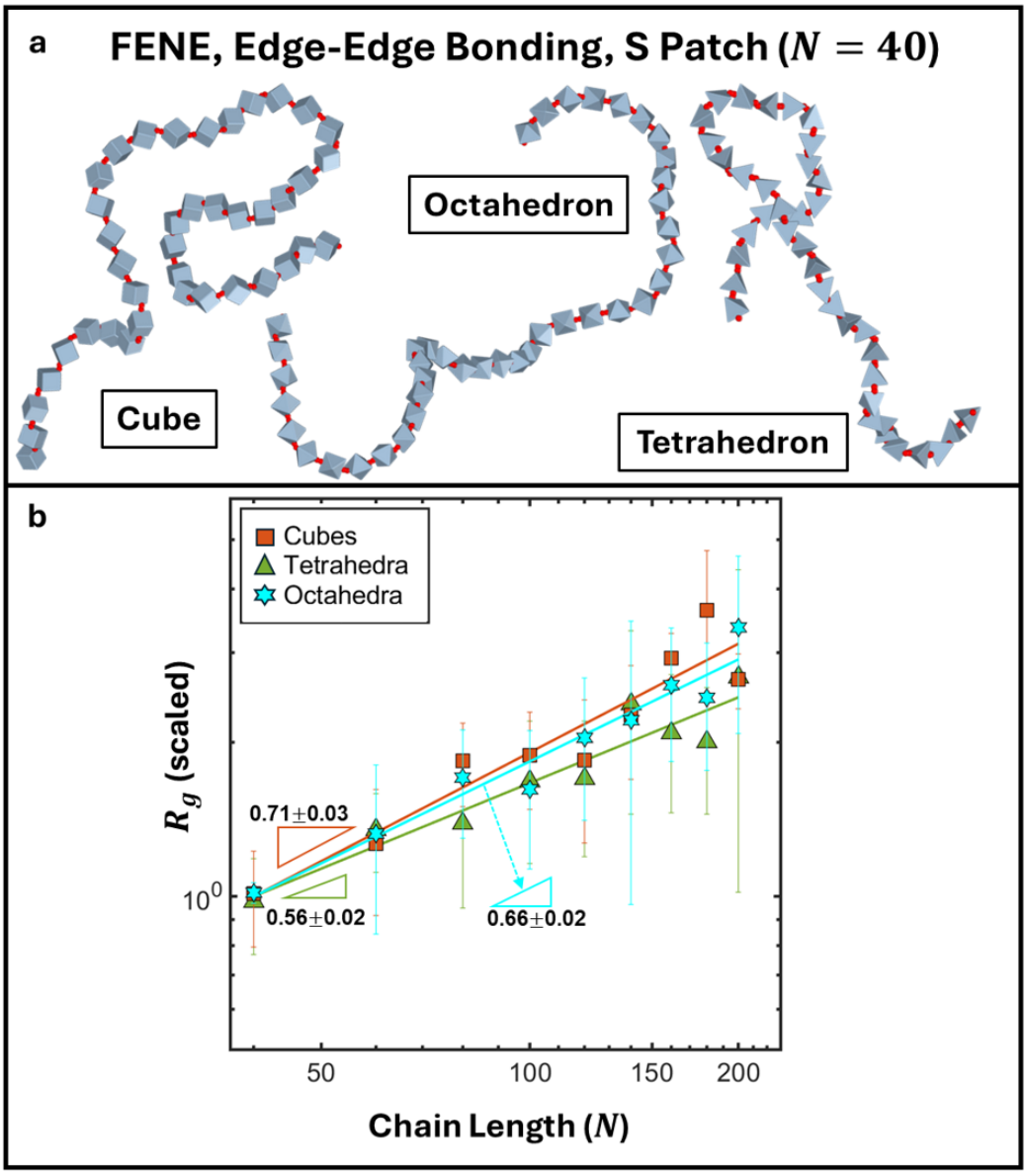

Fig. H1. Polymers with Edge-Edge Bonded Polyhedral Monomeric Subunits. a) Simulation snapshots of edge-edge bonded cubic, octahedral, and tetrahedral NPs using the FENE. b) R_g vs N scaling fits for edge-edge bonded polymeric chain of cubic, octahedral, and tetrahedral NPs.

Appendix I: Scaling Exponent Data from cEBT and Simulations

Table I1. Scaling Exponents from Theory and Simulation

Monomer Geometry	Bond Length (Patch Size)	Bond Type	Bond Potential	Scaling Exponent (Simulation)	Scaling Exponent (Theory)
Tetrahedron	Small	VV	Harmonic	0.58 ± 0.008	0.59
Tetrahedron	Medium	VV	Harmonic	0.58 ± 0.005	0.57
Tetrahedron	Large	VV	Harmonic	0.51 ± 0.007	0.50
Tetrahedron	Small	FF	Harmonic	0.69 ± 0.009	0.67
Tetrahedron	Medium	FF	Harmonic	0.60 ± 0.011	0.61
Tetrahedron	Large	FF	Harmonic	0.51 ± 0.005	0.51
Octahedron	Small	VV	Harmonic	0.58 ± 0.023	0.58
Octahedron	Medium	VV	Harmonic	0.59 ± 0.003	0.55
Octahedron	Large	VV	Harmonic	0.52 ± 0.003	0.52
Octahedron	Small	FF	Harmonic	0.87 ± 0.032	0.90
Octahedron	Medium	FF	Harmonic	0.59 ± 0.001	0.60
Octahedron	Large	FF	Harmonic	0.51 ± 0.003	0.51
Cube	Small	VV	Harmonic	0.62 ± 0.029	0.63
Cube	Medium	VV	Harmonic	0.60 ± 0.011	0.57
Cube	Large	VV	Harmonic	0.53 ± 0.003	0.52
Cube	Small	FF	Harmonic	0.95 ± 0.012	0.91
Cube	Medium	FF	Harmonic	0.59 ± 0.024	0.57
Cube	Large	FF	Harmonic	0.52 ± 0.006	0.52
Tetrahedron	Small	VV	FENE	0.56 ± 0.016	0.55
Tetrahedron	Small	EE	FENE	0.56 ± 0.016	0.56
Tetrahedron	Small	FF	FENE	0.56 ± 0.021	0.53
Octahedron	Small	VV	FENE	0.56 ± 0.015	0.55
Octahedron	Small	EE	FENE	0.61 ± 0.015	0.62
Octahedron	Small	FF	FENE	1.00 ± 0.000	0.97
Cube	Small	VV	FENE	0.60 ± 0.020	0.59
Cube	Small	EE	FENE	0.62 ± 0.020	0.63
Cube	Small	FF	FENE	1.00 ± 0.000	0.96

VV: vertex-vertex, **EE:** edge-edge, **FF:** face-face

References

1 T. Vo and S. C. Glotzer, *Proc Natl Acad Sci U S A*, 2022, **119**, e2116414119.